cosmetics

MDPI

Review

Spectroscopic Evaluation of Chemical and Physical Stability in Cosmetics

Xue-Lin Chen [1,2,†], Tong-Tong Liu [1,†], Xin-Ru Wang [1], Jin Cao [1], Gang-Li Wang [1,*] and Shao-Ming Jin [1,*]

[1] National Institutes for Drug Control, Beijing 100050, China; 3325020807@stu.cpu.edu.cn (X.-L.C.); liutongtong@nifdc.org.cn (T.-T.L.); 202434124@syphu.edu.cn (X.-R.W.); caojin@nifdc.org.cn (J.C.)
[2] School of Traditional Chinese Pharmacy, China Pharmaceutical University, Nanjing 211198, China
* Correspondence: wanggl@nifdc.org.cn (G.-L.W.); jinshaoming@nifdc.org.cn (S.-M.J.)
† These authors contributed equally to this work.

Abstract

Spectroscopy can monitor changes in cosmetics during storage and use, but chemical reactions, droplet scattering, and molecular environments may influence the same signal. This review compares ultraviolet–visible, infrared, near-infrared, Raman, and fluorescence studies of active ingredients, sunscreen performance, color retention, lipid oxidation, and physical instability. Differences among studies are examined in relation to the analytes, sample forms, and reference measurements. Studies of finished products and experimental formulations have recorded changes in selected ingredient contents, ultraviolet absorption by films, color, and physical properties. Raw-material models help investigate reactions, while initial spectra characterize composition and interactions. Studies of carrier protection reported different outcomes, including absorption after irradiation, remaining ingredient content, and encapsulation efficiency. For example, encapsulation efficiency can remain unchanged even when particle properties change. For quantification or quality assessment, spectral measurements should be validated against reference measurements from the same sample batches, with errors evaluated in independent batches. Direct comparisons on the same samples can show whether combining methods improves prediction accuracy or detects changes earlier.

Keywords: cosmetic stability; spectroscopic monitoring; oxidation and photodegradation; physical instability; chemometrics; validation of spectroscopic methods

1. Introduction

Cosmetic stability assessment examines whether ingredient contents, appearance, and performance meet requirements throughout the intended storage period and under specified conditions of use. This review addresses chemical changes and physical instability. Compliance with microbiological limits and preservative efficacy also form part of stability assessment. Neither can be established directly using the spectroscopic methods discussed here. In emulsions, gels, and suspensions, chemical reactions and changes in phase structure may occur together and influence each other. Samples therefore need to be examined over storage or treatment time.

Chemical changes include oxidation, hydrolysis, photoisomerization, and bond cleavage. These processes can consume original ingredients and form reaction products, changing the composition of the formulation [1–4]. Physical changes include flocculation,

Academic Editor: Luis Alfonso Trujillo-Cayado

Received: 30 October 2026
Revised: 21 November 2026
Accepted: 23 November 2026
Published: 25 November 2026

Copyright: © 2026 by the author. Licensee MDPI, Basel, Switzerland. This article is an open access article distributed under the terms and conditions of the Creative Commons Attribution (CC BY) license.

coalescence, ripening, creaming, and crystallization, which alter droplet distributions, phase structure, or local composition [5–7]. Chemical reactions and physical changes can produce similar shifts in the baseline, absorbance, or peak intensity. The same spectral change can therefore have more than one explanation.

Chromatography and chromatography coupled with mass spectrometry can quantify ingredients and identify degradation products. Particle sizing, rheology, and microscopy are used to examine physical changes. Ingredient analysis in complex formulations usually requires extraction or separation [8,9]. Spectroscopy can often simplify sample preparation and facilitate continuous or repeated measurements. However, it also records matrix and scattering effects, whose contributions must be distinguished from those of the target ingredient.

This review distinguishes evidence from finished products, experimental formulations, and raw-material models. Finished-product tests describe storage or use under specified conditions, whereas ingredient solutions and carrier models facilitate the analysis of reactions and interactions. Particular attention is given to tracking ingredient content, examining physical changes in emulsions, and identifying local crystallization, together with the validation requirements for these measurements.

Guo et al. [8] and Celeiro et al. [9] mainly reviewed sample preparation and analytical methods for quality and safety testing. Zhao et al. [10] focused on Raman applications in skin analysis, efficacy assessment, and quality control. Li et al. [11] also reviewed ingredient detection and transdermal mechanisms, including selected photostability applications. The present review focuses on how spectral changes after storage or irradiation relate to actual changes in the product. For example, reduced absorption may reflect ingredient loss or scattering effects; content or particle-size measurements can help distinguish these contributions. Studies addressing similar questions are compared in terms of formulation, treatment conditions, and measurement configuration. The review also considers whether combining spectroscopic methods provides additional information.

PubMed and Web of Science were searched for the relevant literature published between January 2000 and October 2026. The final literature search was completed in October 2026. Search terms combined three themes: study materials, spectroscopic methods, and stability. The material terms covered cosmetics, personal care products, sunscreens, and cosmetic ingredients. The method terms covered ultraviolet–visible, infrared, near-infrared, Raman, and fluorescence spectroscopy. Stability terms included storage, aging, degradation, oxidation, photostability, and physical instability. Priority was given to studies using these methods to examine changes in finished cosmetics, experimental formulations, or relevant ingredients during storage, irradiation, heating, or related treatments. Articles unrelated to the selected techniques or cosmetic stability, or lacking sufficient experimental information to support the analysis, were excluded. Studies reporting only initial spectra were discussed as initial characterization when they helped explain formulation compatibility or subsequent stability results. Studies in food and other systems were included for methodological comparison, while reviews and established methodological papers provided background. Earlier publications relevant to measurement principles or signal interpretation were included as supplementary sources outside the stated publication period. The review cites 79 references, comprising stability studies, initial characterization, methodological studies in other systems, background reviews, and method papers.

2. How Chemical and Physical Changes Affect Spectra

Interpreting spectra collected after storage or irradiation first requires distinguishing the chemical reactions and physical changes that may have occurred. Figure 1 summarizes the links between chemical or physical changes, spectral responses, and reference measurements.

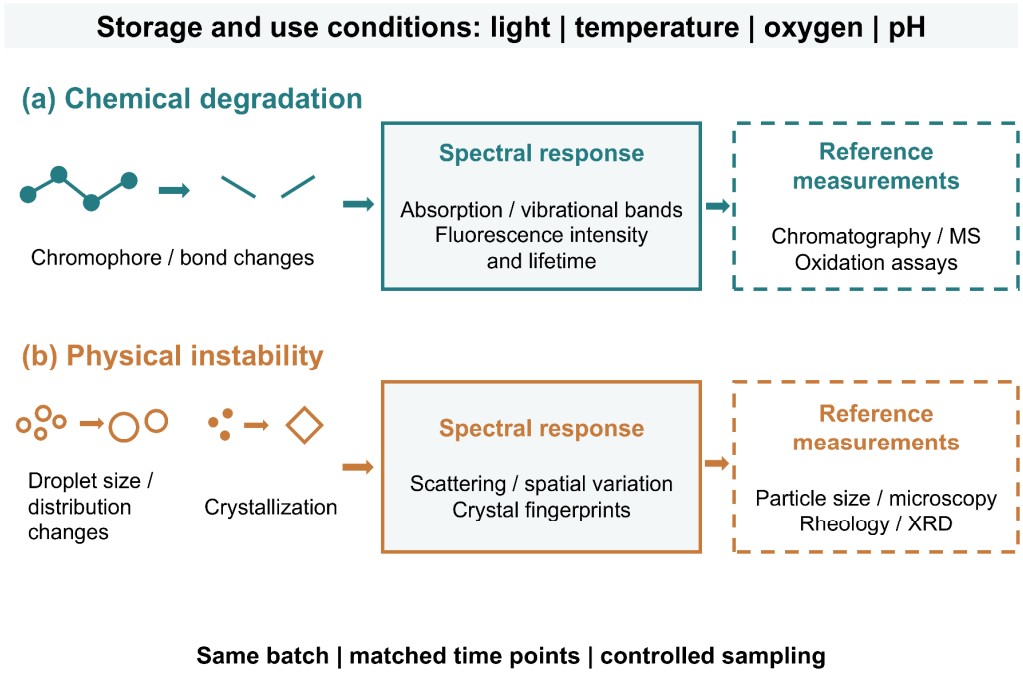

Figure 1. Chemical degradation, physical instability, and their potential effects on spectral measurements. Panel (**a**) shows chemical degradation and associated spectral responses; panel (**b**) shows physical instability, including changes in droplet size or distribution and crystallization. Solid arrows connect sample changes, spectral responses, and reference measurements; dashed boxes list reference methods. Molecules, droplets, and crystals are schematic. The signals observed depend on the formulation and treatment conditions. MS, mass spectrometry; XRD, X-ray diffraction.

2.1. Chemical Degradation and Molecular Spectral Changes

Oxidation, hydrolysis, and photoisomerization can deplete the original compounds and generate reaction products. Changes in conjugation affect ultraviolet–visible absorption, while the formation or loss of functional groups alters infrared and Raman bands. Fluorescence is sensitive to the state of emitting molecules and their surroundings. Time-dependent spectral changes have been observed in studies of emulsions, sunscreens, free fatty acids, and retinol in carriers [1–5,12]. Inclusion complexation, aggregation, and scattering may also alter the same measurement. Where signals overlap strongly or band assignments are uncertain, chromatography, mass spectrometry, nuclear magnetic resonance (NMR), or chemical assays can aid interpretation.

2.2. Spectral Changes Associated with Droplet Changes and Crystallization

Emulsion destabilization alters droplet size and distribution through several processes. Flocculation forms droplet clusters without necessarily merging the droplets, whereas coalescence merges them. During Ostwald ripening, dispersed-phase material moves through the continuous phase from smaller to larger droplets, causing the former to shrink and the latter to grow. Creaming and sedimentation mainly alter droplet concentrations at different sample heights. These changes affect scattering and thereby alter transmission or apparent absorbance. Wavelength, concentration, and sampling height also affect the signal, so increased absorbance alone cannot distinguish the specific destabilization process [6]. Crystallization may additionally alter local vibrational spectra. In an emulsion-aging study, Fourier-transform infrared (FTIR) spectroscopy helped interpret chemical changes, whereas conductivity and other measurements were more sensitive to some physical changes [5].

2.3. Limitations of Optical Measurements for Microbial Assessment

Optical measurements such as turbidity are insufficiently selective for microbial growth. In a film-forming gel study, turbidity at 600 nm showed no significant change over 28 d, yet culture tests detected microbial growth in the unsterilized honey aromatic water [13]. Color and pH can also change for reasons unrelated to microbial growth. Compliance with microbiological limits should be assessed using appropriate microbiological tests, including culture-based enumeration. Preservative efficacy requires a separate efficacy test.

3. Applications and Limitations of Ultraviolet–Visible Spectroscopy

Ultraviolet–visible (UV–Vis) spectroscopy is used to estimate ingredient content, measure ultraviolet absorption by sunscreen films, and assess color (Table 1). For content measurements, the signal must be selective for the target compound; when extraction is required, recovery must also be checked. In intact samples, droplet scattering can affect apparent absorbance, and film thickness and uniformity can affect sunscreen measurements.

3.1. Active Ingredient Content and Functional Colorimetric Assays

Vitamin C absorption changes with both degradation and acid–base speciation. Ahmad et al. [1] tracked ascorbic acid photolysis in creams using absorption at 245 nm and detected dehydroascorbic acid and 2,3-diketogulonic acid. The photolysis rate varied with pH, emulsifier and humectant type, and viscosity [1]. Oxidation alters the electronic structure of ascorbic acid, and the resulting dehydroascorbic acid can subsequently undergo hydrolytic ring opening. When comparing the amount remaining in different formulations, the pH of the measurement medium should be controlled. Otherwise, absorption differences caused by acid–base speciation may be counted as ingredient loss.

Binding to a carrier can also shift absorption maxima. In a chitosan–vitamin C complex, the absorption maximum shifted from 245 to 247 nm, accompanied by changes in amino- and hydroxyl-related FTIR bands. The authors attributed these changes to electrostatic interactions [14]. If the complex is quantified using a calibration established for free ascorbic acid, the effect of this shift on the content estimate should be checked. A carboxymethyl cellulose–nanohydroxyapatite composite showed smaller losses of ascorbic-acid-related absorption after sunlight exposure and heating. Changes after laser irradiation depended on the laser conditions [15]. Comparisons therefore need to account for the light source, exposure conditions, and treatment duration.

Studies of encapsulated retinol and retinoic acid have also used post-irradiation absorption to assess carrier effects. A fatty acyl amide–β-cyclodextrin vesicle study estimated the remaining retinol after ethanol extraction [16]. Retinoic acid lipid carriers, including systems supplemented with inorganic sunscreen agents, were measured after dissolution in methanol and compared with free retinoic acid in methanol [17]. Both studies observed smaller absorption losses in the encapsulated systems. In both studies, the spectra were recorded in solvent rather than in the original dispersions.

Several ingredients can contribute to absorption in a finished product, and estimating a single compound differs from estimating an extract. Coenzyme Q10 in an inclusion-complex serum was quantified at 276 nm using a formulation blank and dilution controls. The measured content, appearance, viscosity, and pH changed little during storage at room temperature in the dark [18]. A sunscreen cream containing phytosomes of Viola tricolor extract also used absorption to estimate the amount remaining at different temperatures [19]. The former measurement targeted a defined compound, whereas the latter included several absorbing constituents. Retention of the extract's overall absorption therefore does not imply unchanged amounts of every constituent.

Another study of α-lipoic acid lipid carriers used UV–Vis for characterization after preparation and high-performance liquid chromatography (HPLC) to measure the amount remaining at set intervals. After 120 d of natural sunlight exposure, retention was approximately 88.5% in the carrier group and 0.7% for the free compound in methanol. The carrier thus reduced α-lipoic acid loss under these conditions [20].

DPPH (2,2-diphenyl-1-picrylhydrazyl) and ABTS (2,2′-azinobis(3-ethylbenzothiazoline-6-sulfonic acid)) colorimetric assays measure absorption changes in the DPPH radical and ABTS radical cation, respectively. They assess radical-scavenging capacity under the in vitro assay conditions [21,22], rather than directly measuring oxidation within the product. A phycocyanin skin cream showed a greater decline in in vitro radical-scavenging capacity at higher storage temperatures, together with changes in physical properties [23]. These measurements recorded both functional and physical changes but did not attribute them to degradation of a specific ingredient. Over a 15 d test, composite tea tree oil microcapsules showed a slower decline in DPPH and ABTS radical-scavenging capacity than free tea tree oil. Release was also more gradual than from complex coacervate capsules [24]. Release rate affects the amount of material available to react, so a slower decline in scavenging capacity may reflect both ingredient retention and release behavior. Comparisons should therefore consider the amount released into the assay, alongside color, turbidity, and reaction time.

3.2. Photostability of Sunscreen Systems

The spectrum of an intact sunscreen film measures how much ultraviolet radiation is transmitted or absorbed. Analysis of an irradiated sample can answer a different question: which filters remain and what products have formed? Commercial sunscreens and filter combinations showed changes in absorption after irradiation [25,26], and Dondi et al. [2] identified dimers and cross-adducts. Freitas et al. [27] extracted and diluted irradiated films and measured the ratio of mean absorbance in the ultraviolet A and ultraviolet B regions (UVA/UVB). The ratio remained relatively high even though HPLC showed losses of some filters and antioxidants [27]. The ratio thus described the balance of absorption between the two bands in the extract; it did not measure protection by the intact film. In separate model mixtures, the authors also detected photoproducts by gas chromatography–mass spectrometry (GC–MS) [27].

Interactions between filters can affect their behavior after irradiation [3,26]. HPLC measurements showed that adding diethylamino hydroxybenzoyl hexyl benzoate (DHHB) did not improve avobenzone retention after UVA exposure in the tested emulsion [28]. In formulations containing passion fruit seed and paracress extracts, ultra-high-performance liquid chromatography (UHPLC) also detected losses of active ingredients after temperature cycling [29]. Adding a UV-absorbing ingredient does not ensure greater retention of other ingredients after light or temperature treatment.

Assessment of a carrier depends on the endpoint measured. One emulgel study examined octyl methoxycinnamate (OMC), also known as ethylhexyl methoxycinnamate (EHMC), encapsulated in poly(lactic acid) (PLA). After irradiation, the authors compared the cis- and trans-isomer peak areas by HPLC and found less photoisomerization in the encapsulated group. They used transmission spectra to estimate the in vitro sun protection factor (SPF) [30]. In emulsions containing silica-encapsulated filters, UV–Vis measurements of films on poly(methyl methacrylate) (PMMA) plates were used to calculate spectral areas and in vitro SPF before and after irradiation. FTIR was used to examine filter distribution in the stratum corneum and retention at the skin surface [31]. The former study distinguished isomers, whereas the latter primarily described the film's overall optical behavior after irradiation.

In a study of avobenzone-loaded nanostructured lipid carriers (NLCs), post-irradiation measurements mainly concerned absorption, while HPLC was used in a separate release experiment [32]. A comparison of liposomes, NLCs, and solid lipid nanoparticles (SLNs) used the ratio of UVA absorption areas after and before irradiation [33]. Studies of mesoporous silica MCM-41 and hydrotalcite compared irradiation effects using solid-state diffuse reflectance spectra and separately measured release from formulations [34,35]. None of these optical comparisons directly measured the amount of filter remaining after irradiation.

The same carrier may have opposite effects on different guest molecules. Several cyclodextrin inclusion studies observed smaller absorption losses after filter irradiation [36–39]. However, a γ-cyclodextrin polymer slowed EHMC absorption loss while accelerating signal loss from avobenzone or curcumin [40]. Different filters in MCM-41 likewise showed decreased, largely unchanged, or increased absorption [41]. Kuroda et al. [42] combined HPLC and NMR to distinguish the effects of inclusion complexation, aggregation, and keto–enol equilibria on absorption.

Results for the same filter may also differ between measurement configurations. Holt et al. [43] found that absorption and protection-factor changes differed between dilute solutions and more concentrated oil-phase models. Scalia et al. [44] compared spectrophotometric and HPLC results obtained using different substrates. Akrman et al. [45] examined the effects of quartz roughness and sample application on in vitro measurements of commercial products. Comparisons of SPF or the UVA protection factor (UVA-PF) should therefore specify the substrate and how the sample was applied when measurements are made on films.

Storage assessment of sunscreen formulations also requires measurements of ingredient content, physical properties, and sunscreen performance. Sharma Bora et al. [46] studied three batches of sunscreen cream, comparing content, pH, rheology, droplet diameter, and in vitro SPF calculated from ethanol-diluted samples. FTIR was used both for compatibility analysis during preparation and for comparison of spectra before and after storage. Together, these measurements assessed the formulation after 6 months at 40 ± 2 °C and 75 ± 5% relative humidity [46]. An avobenzone microsponge gel study examined appearance, pH, viscosity, content, and release during storage, with no marked changes in these endpoints. FTIR and differential scanning calorimetry (DSC) of the microsponges mainly served for characterization after preparation [47].

3.3. Color Retention in Dyes and Pigments

Color and colorant content do not necessarily change together. Color differences and visible reflectance describe appearance, whereas absorption after extraction can estimate target colorant content. Carminic acid showed a gradual decrease in visible absorption under strongly alkaline conditions. Heating and oxidizing or reducing atmospheres also altered some absorption peaks [48]. These changes involve the chromophore or its state, but absorption spectra alone cannot establish the structures of the products.

A modified-palygorskite Pickering emulsion study estimated the remaining natural colorant from absorption after extraction [49]. A chitosan–palygorskite/sappanwood hybrid pigment study assessed color retention after light and thermal aging using color differences [50]. A hydrophobic layered double hydroxide (LDH) pigment study compared color differences after simulated light exposure [51]. All three examined the effects of carriers or surface treatment on color retention. However, the first measurement more closely reflected extracted colorant content, whereas the latter two were also affected by particle shielding, scattering, and wetting.

When pigment powders are incorporated into color cosmetics, particle distribution and film structure further affect optical measurements. Studies of zein/LDH hybrid

pigments and nail polish containing algal pigments mainly used colorimetry or visible reflectance to assess color after storage or treatment. Initial UV–Vis and FTIR spectra were used to examine composition and interactions [52,53].

Color comparisons require control of pH, substrate, film thickness, wetting, and measurement geometry as appropriate for the sample form. Irradiation studies also require a consistent light dose. To investigate whether the colorant itself has changed, the extracted colorant can be examined by chromatography or mass spectrometry. Vibrational bands with established assignments can provide additional structural evidence.

3.4. Transmission and Scattering Measurements of Physical Changes

Celis and Garcia-Rubio [6] estimated droplet-size distributions in dilute oil-in-water (O/W) model emulsions using transmission spectra from 300 to 820 nm and a scattering model. A fragrance-capsule emulsion study recorded early backscattering changes along the sample height using multiple light scattering to examine differences in spatial distribution [54]. In a retinol hydrogel, backscattering changed little during the first 6 h after preparation, although microscopy already showed a lower proportion of small droplets [55]. Here, microscopy revealed a change in the droplet population that was not apparent in the bulk measurement.

Diluting a cream to measure transmission can disrupt droplet clusters. A shorter optical path or diffuse reflectance allows the undiluted sample to be examined. Microscopy, hydrodynamic particle size measured by dynamic light scattering (DLS), and the polydispersity index (PDI) can help interpret the optical changes.

Table 1. Main findings from UV–Vis and light-scattering studies.

Study Purpose	Samples and Conditions	Main Findings	Reference Measurements and Controls	Scope and Limitations
Dynamic: active ingredient photolysis [1]	Ascorbic acid cream; light exposure	Absorption at 245 nm decreased; photolysis rate varied with formulation conditions	Comparisons of pH, emulsifiers, and humectants; thin-layer chromatography for product identification	Absorption also depends on ascorbic acid acid–base speciation
Irradiated vs. unirradiated: sunscreen film extracts [27]	Formulation films extracted and diluted after irradiation; separate model mixtures of active ingredients	UVA/UVB mean absorbance ratio remained relatively high after irradiation	Formulations: HPLC; separate models: GC–MS	Relative UVA versus UVB absorbance in the extract; individual filter retention was assessed by HPLC
Dynamic: colorant changes [48]	Carminic acid; strong alkali, heating, and different atmospheres	Visible absorption decreased under strong alkali; heat and atmosphere treatments altered some peaks	Comparison of treatment conditions	Absorption changes alone cannot identify product structures
Dynamic: droplet changes [55]	Retinol hydrogel; first 6 h after preparation	Backscattering changed little	Microscopy	The proportion of small droplets had already decreased in micrographs
Dynamic: antioxidant function [24]	Composite tea tree oil microcapsules; 15 d test	DPPH radical and ABTS radical cation absorption changes [21,22]; scavenging capacity declined more slowly than in the free-oil group	Free tea tree oil and complex coacervate capsule controls; release test	Release rate also affects measured scavenging capacity

Note: In Tables 1–4, Dynamic denotes repeated optical measurements over time, including at least one intermediate time point. Before-and-after denotes measurements made before treatment and at its endpoint. Irradiated vs. unirradiated denotes a comparison with a separate unexposed control. Post-aging only denotes characterization of a change observed after aging. Initial denotes

characterization of the starting material, formulation, or model system. Other systems identifies studies included for methodological comparison.

Table 2. Main findings from FTIR and NIR studies.

Study Purpose	Samples and Conditions	Main Spectral Findings	Reference Measurements and Controls	Scope and Limitations
Dynamic: emulsion aging (FTIR) [5]	O/W emulsions; 12 months at 0–50 °C	Unsaturation index at 3006 cm^{-1} decreased and carbonyl index at 1746 cm^{-1} increased in some systems	Conductivity, viscosity, pH, and texture	Carbonyl region includes original esters and aging products; band enhancement alone cannot quantify new oxidation products
Before-and-after: liposome irradiation (ATR-FTIR) [56]	Sargassum-derived liposome dispersions; irradiation with a 75 W xenon lamp for 30 min; samples collected before and after irradiation were freeze-dried for ATR-FTIR measurements	Main lipid bands, including 2919 and 2849 cm^{-1}, changed little	GC–MS before/after irradiation; coating controls; separate particle-size and zeta-potential measurements after 28 d at 4 °C	Spectra collected after brief irradiation and freeze-drying; dispersion particle sizes came from a separate storage experiment
Dynamic: polymer aging (FTIR) [57]	Cosmetic polyether polyurethane; ethanol–water 80/20, 60 °C, 4 weeks	Ether-related signals decreased; urethane carbonyl changes were small	Molecular weight, NMR, viscosity, and mechanical properties	Accelerated testing of a raw-material polymer
Dynamic: packaging and storage (FT-NIR) [58]	Commercial face cream; five packaging types; room or refrigerated temperature for 2 and 4 months	PCA revealed some storage and packaging differences; PLS1 related spectra to color	L*, a*, and ΔE* measurements	Grouping alone cannot determine the causes of change
Other systems: oxidation prediction (NIR) [59]	Food O/W emulsion with 20% (v/v) fish oil; iron-induced oxidation	PLSR predicted conjugated diene values; prediction R^2 = 0.996; error = 7.26 mmol eq. LH/kg oil	Conjugated diene values measured after extraction and compared with model predictions	Results apply to the tested food emulsion system
Initial: compatibility (ATR-FTIR) [60]	Ferulic acid–excipient mixtures; spectra collected after mixing	Measured and theoretically summed spectra differed in peak positions, band shapes, and correlation	TG/DTG and DSC	Storage was not tracked

Table 3. Main findings from Raman studies.

Study Purpose	Samples and Conditions	Main Spectral Findings	Reference Measurements and Controls	Scope and Limitations
Dynamic: photodegradation tracking [61]	Retinol in an oil phase, 0.003–0.3 mol/L; ultraviolet irradiation	Retinol and product bands tracked; UVA/UVB differences depended on initial concentration; aeration accelerated degradation	Light-source, oxygen-exposure, and additive controls	Results apply to the tested oil-phase models and irradiation conditions
Dynamic: formulation irradiation [62]	Formulations containing β-carotene with or without vitamins C and E; Raman measurements before UV exposure and after multiple exposure durations up to 300 s	Resonance Raman measured remaining carotenoids	Different formulation combinations	Measurements targeted carotenoids
Post-aging only: identification of crystalline deposits [7]	Anhydrous foundation with metal oxides; approximately 2 months of aging	Raman at 532 nm detected avobenzone-related signals in deposits	PXRD, SEM/EDS, FTIR, and raw-material controls	Endpoint identification after aging; the precise structure of the crystalline deposits remained unresolved

Other systems: fatty acid oxidation [4]	Free fatty acids; simulated solar ultraviolet irradiation	CH_2/CH_3 intensity ratio and ratios of bands at 1165/1640 and 1730/1640 cm^{-1} compared	Before/after irradiation controls; FTIR	Band-ratio interpretation is limited to the fatty acid models used
Initial: content prediction [63]	PE hydrogels; 0.4–8.3% (w/w); 96 samples	Raman–PLSR; RMSEP = 0.148% (w/w)	64 training and 32 test samples	No repeated spectra during storage; degraded samples were not tested
Initial: compositional characterization [64]	1% caffeine nanoemulsion; 90 d at 5 and 25 °C; separation in less than 7 d at 45 °C	Initial Raman spectra at 785 nm	Appearance, pH, DLS/PDI, zeta potential, and ripening analysis	No repeated spectra during storage; changes assessed by appearance and physical-property tests

Note: The listed wavenumbers are band positions; band-intensity ratios are dimensionless.

Table 4. Main findings from fluorescence studies.

Study Purpose	Samples and Conditions	Main Spectral Findings	Reference Measurements and Controls	Scope and Limitations
Before-and-after: melatonin encapsulation efficiency [65]	Melatonin transfersomes and niosomes; six cycles of 24 h each at 4 and 45 °C	Excitation at 274 nm, emission at 370 nm; encapsulation efficiency did not change significantly	DLS, PDI, and zeta potential; HPLC comparison in the supplementary material of Ref	Encapsulation efficiency describes the fraction encapsulated, not the total amount remaining
Dynamic: liposome irradiation [12]	Retinol liposomes; excitation at 374 nm; ultraviolet irradiation at 312 nm	Without cholesterol, BHT increased initial lifetime, but mean lifetime decreased faster after irradiation	Bulk lifetime, FLIM, and membrane-composition controls	Lifetime cannot be directly converted into remaining content
Initial: filter interactions in methanol [28]	Avobenzone/DHHB in methanol; formulation separately exposed to 27.5 J/cm^2 UVA	Emission intensity decreased; lifetime remained largely unchanged	Formulation UVA/UVB absorbance ratio, HPLC, and dark controls	No increase in post-irradiation avobenzone retention measured by HPLC in the tested formulation
Dynamic: intercalated-material irradiation [66]	PABA/anionic clay; excitation and irradiation at 297 nm	Emission intensity decreased during irradiation	Free versus intercalated samples; X-ray diffraction (XRD), TG, and release tests	Results concern the intercalated material
Other systems: oxidation-related fluorescence [67,68]	Aldehyde–amino acid models; extracts of frozen-stored sardines	Model emission depended on aldehyde structure and combinations; aqueous sardine-extract fluorescence ratio correlated with TBA index	Aldehyde–amino acid combination controls [67]; TBA and other quality indicators [68]	Results from model reactions and fish storage
Dynamic: ROS probe [69]	TiO_2 and lignin/TiO_2 ingredients; sunlight exposure for 20–100 min	Emission near 460 nm; kraft lignin/TiO_2 gave lower signals than pure TiO_2 and alkali lignin/TiO_2	Comparison of TiO_2, lignin, and their composites	Results limited to the probe system with candidate ingredients

4. Infrared and Near-Infrared Spectroscopy

4.1. Spectral Regions and Sampling

Mid-infrared (MIR; 4000–400 cm^{-1}) spectra mainly record fundamental molecular vibrations. FTIR is commonly used to collect functional-group and fingerprint-region

information [70]. Attenuated total reflectance (ATR) facilitates direct measurements of creams or films, but crystal contact, pressure, and surface composition affect the results. Near-infrared (NIR; 780–2500 nm) spectra mainly record O–H, C–H, and N–H overtones and combination bands, which are broad and overlap extensively. Diffuse reflectance and fiber-optic probes are common sampling approaches. MIR is often used to interpret structural changes, whereas NIR facilitates rapid measurements of samples without extraction. NIR can also predict content or oxidation indices through models calibrated against measured values.

4.2. Oxidation and Degradation During Storage and Treatment

Masmoudi et al. [5] stored five O/W emulsions at 0–50 °C for 12 months. In some formulations, the unsaturation index at 3006 cm^{-1} decreased and the carbonyl index at 1746 cm^{-1} increased; deconvolution of the carbonyl region also revealed changes in overlapping bands. A decrease in the olefinic =C–H stretching band near 3006 cm^{-1} is consistent with a loss of unsaturated structures. The carbonyl region, however, includes contributions from the original lipid ester groups, aging products, and changes in the local environment. An increase in the overall band at 1740–1750 cm^{-1} cannot therefore be attributed entirely to newly formed aldehydes and ketones. Together with the physical-property measurements, these changes support lipid oxidation in some emulsions. Figure 2 summarizes related signals reported in lipid oxidation studies.

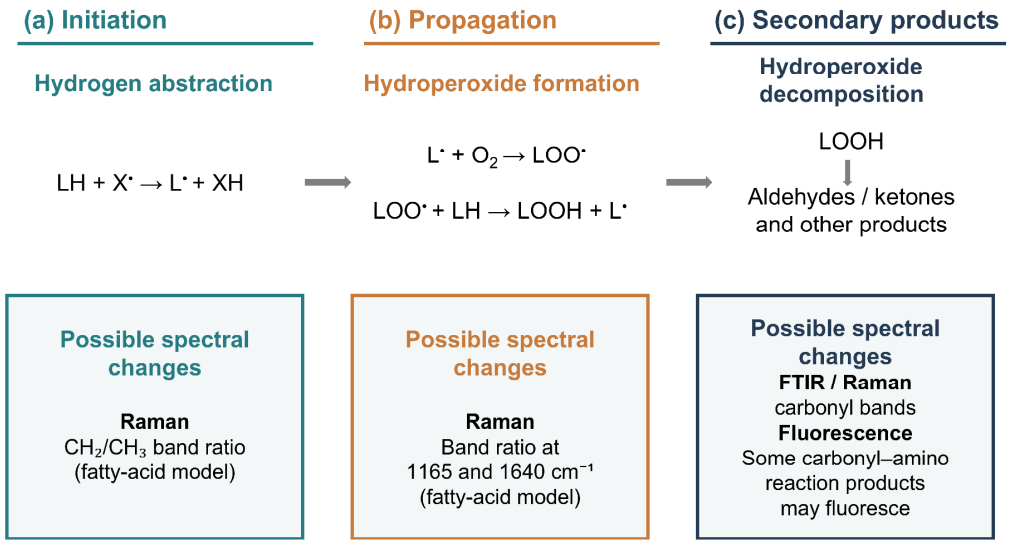

Figure 2. Lipid oxidation processes and possible spectral changes, summarized from studies [4,5,67,68]. Panels (a–c) show initiation by hydrogen abstraction, propagation involving hydroperoxide formation, and hydroperoxide decomposition leading to secondary products, respectively. Oxidation processes can overlap, and the order of spectral changes can vary between formulations. The Raman band ratios shown were reported for specific fatty-acid models. Carbonyl bands may include contributions from pre-existing ester groups as well as oxidation products. LH, lipid; L•, lipid radical; LOO•, lipid peroxyl radical; LOOH, lipid hydroperoxide. X• abstracts a hydrogen atom from LH to form XH.

Cruz-Lugo et al. [56] briefly irradiated Sargassum-derived liposomes and fucoidan-coated systems, then freeze-dried samples collected before and after irradiation for ATR-FTIR measurements. The main lipid bands changed little. In a separate storage experiment at 4 °C for 28 d, particle size, PDI, and zeta potential changed in some systems [56].

Kim et al. [57] stored a cosmetic polyether polyurethane in ethanol–water (80/20, v/v) in sealed vials containing air at 60 °C for 4 weeks. Ether-related signals decreased, whereas changes in urethane carbonyl signals were relatively small. Decreases in molecular weight, viscosity, and mechanical properties, together with ester bonds detected by NMR, supported oxidative chain scission. Changes in this polymer mainly involved ether segments, unlike the enhanced carbonyl signals in the emulsion study [5]. Thus, even during aging, the direction of band changes depends on the composition and reaction sites.

The surrounding medium may also alter sunscreen-particle surface structures. Virkutyte et al. [71] treated a commercial TiO_2 sunscreen emulsion and coated particles with simulated chlorinated swimming-pool water. ATR-FTIR showed changes in bands associated with carboxylates, O–H, and Al–O/Ti–O–Al. X-ray photoelectron spectroscopy (XPS), transmission electron microscopy (TEM), and zeta-potential measurements supported damage to the protective coating. Radical-probe and p-chlorobenzoic acid degradation experiments in the coated raw-particle model also indicated increased photocatalytic activity after treatment [71].

4.3. Initial Structure and Formulation Compatibility

Compatibility screening during preparation can help with excipient selection. Bezerra et al. [60] first identified unusual thermal behavior in ferulic acid–excipient mixtures using thermogravimetry and derivative thermogravimetry (TG/DTG) and DSC. They then compared measured ATR-FTIR spectra with theoretical sums of the individual-component spectra [60]. Differences in peak position, band shape, and correlation may result from reactions, phase changes, or altered hydrogen bonding and need to be interpreted alongside thermal analysis.

A hydroxyethyl cellulose (HEC) serum study used FTIR to examine component interactions and compared post-application skin hydration for samples before and after 7 d of storage at room temperature [72]. An EHMC gel study used FTIR, Raman spectroscopy, and rheology to characterize initial structure, with temperature treatments and centrifugation tests to assess short-term physical stability [73]. Vibrational bands mainly reflect local interactions, whereas rheology describes the formulation's bulk mechanical behavior. Skin hydration measurements assess moisturizing performance after application, while centrifugation tests examine the formulation's physical state under stress.

4.4. Near-Infrared Assessment of Storage Changes and Prediction of Quality Indicators

Gliszczyńska-Świgło et al. [58] stored a commercial face cream in five packaging types at room and refrigerated temperatures for 2 and 4 months. Principal component analysis (PCA) of Fourier-transform near-infrared (FT-NIR) spectra revealed differences associated with storage time and some packaging types. Single-response partial least squares regression (PLS1) separately related FT-NIR spectra to L*, a*, and total color difference, ΔE* [58]. The spectra distinguished some storage conditions and were associated with changes in color [58]. They did not identify the cause. Measurements of mass loss, moisture content, or droplet size could help distinguish changes in the emulsion from losses during storage.

NIR spectra can predict an oxidation indicator after calibration against values obtained using a reference method. Daoud et al. [59] induced oxidation with iron in a food O/W emulsion containing 20% (v/v) fish oil. NIR spectra were collected directly from the undiluted emulsion, and conjugated diene values measured after extraction were used to develop a partial least squares regression (PLSR) model. Calibration and prediction R^2 values were 0.967 and 0.996, respectively, with a prediction error of 7.26 mmol eq. LH/kg oil and a relative error of 7.8% [59]. Unlike storage grouping and color associations in face

cream [58], this study provided a defined oxidation indicator for spectral prediction. These errors nevertheless apply to the food emulsions studied. Performance needs to be checked with new samples when the oil phase, emulsifier, or oxidation conditions change.

4.5. Applicability and Measurement Considerations

Strong mid-infrared absorption in aqueous samples can obscure weak signals, while ATR contact and sampling location affect surface measurements. NIR is susceptible to scattering from droplets, pigments, and packaging. Baseline correction and normalization can reduce some differences, but may also remove information about physical changes when the baseline itself reflects emulsion scattering. Raw spectra should therefore be retained, and preprocessing choices assessed against content or physical-property measurements. Table 2 summarizes the FTIR and NIR studies discussed in this section.

5. Raman Spectroscopy

5.1. Measurement Characteristics and Content Determination

Raman signals arise from inelastic scattering and are sensitive to conjugated C=C bonds, aromatic rings, and some symmetric vibrations, complementing infrared measurements [74]. The water background is generally weak in the fingerprint region, which facilitates measurements of aqueous samples. Emulsion scattering, pigment absorption, and extract fluorescence can still interfere. At trace concentrations, a component may go undetected because its bands overlap with those of more abundant ingredients or are masked by fluorescence. A distinct Raman band can help identify a component whose UV–Vis absorption overlaps with that of other ingredients. Resonance excitation can strengthen the Raman signal of selected compounds. A missing band, however, is not evidence that the component is absent.

Elderderi et al. [63] developed a Raman–PLSR model using 96 hydrogels containing nanoencapsulated piperonyl esters (PE; 0.4–8.3%, w/w). Of these, 64 samples were used for training and 32 for testing. The root mean square error of prediction (RMSEP) was 0.148% (w/w) [63]. The reported error applies to freshly prepared hydrogels. Raman spectra were not collected during storage or irradiation. Testing aged samples would show whether degradation products or changes in the formulation affect prediction accuracy.

5.2. Photochemical and Oxidative Degradation of Active Ingredients

Failloux et al. [61] compared the effects of ultraviolet irradiation, oxygen exposure, and additives on retinol in an oil phase. The difference between UVA- and UVB-induced degradation depended on initial concentration. UVA caused more pronounced degradation at 0.03 and 0.3 mol/L, whereas the rates were similar at 0.003 mol/L. Aeration accelerated degradation. A UVA filter slowed retinol loss, while butylated hydroxytoluene (BHT) reduced the number of photoproduct species detected. The study tracked retinol, retinal, and anhydrovitamin A. Bands at 1606 and 1629.5 cm^{-1} were associated with an electrocyclized retinoid and a deconjugated oxidation product, respectively. Multiple bands provided information on both depletion of the original compound and formation of different products.

Applying band assignments from an oil-phase model to creams also requires consideration of heterogeneous ingredient distribution, scattering, and fluorescence background. Dark controls, formulation blanks, and chromatographic product analysis can help distinguish photoreaction signals from matrix interference.

Darvin et al. [62] used resonance Raman spectroscopy to measure carotenoids in formulations and compared the amounts remaining after irradiation in combinations of

β-carotene and vitamins C and E. This study more closely represented antioxidant changes within formulations than the oil-phase retinol model [61], but the measurements still targeted compounds with the relevant Raman signals. Differences between groups may reflect β-carotene consumption, the effects of other antioxidants, and phase distribution. Remaining amounts alone cannot distinguish the contribution of each process.

5.3. Crystallization and Phase Distribution

Raman microspectroscopy can identify local crystallization. Goral et al. [7] studied an anhydrous foundation containing avobenzone, TiO_2/ZnO, pigments, and waxes, in which white crystals appeared after approximately 2 months of aging. Raman measurements at 532 nm, powder X-ray diffraction (PXRD), scanning electron microscopy (SEM), and energy-dispersive X-ray spectroscopy (EDS) showed that the deposits contained avobenzone together with wax and inorganic constituents. The authors discussed possible involvement of metal oxide surfaces in nucleation and used computational analysis to propose an explanation for crystallization inhibition by ascorbyl palmitate [7]. The precise structure of the precipitated crystals remained unresolved. These measurements identified the composition of local crystals after aging. Because point measurements may miss local crystals, sampling locations and mapping coverage should be reported.

Other studies collected Raman spectra only after preparation. Freire et al. [64] measured initial Raman spectra of caffeine nanoemulsions. Changes during 90 d of storage at 5 and 25 °C were assessed mainly by appearance, DLS/PDI, zeta potential, and ripening analysis; samples at 45 °C separated in less than 7 d [64]. Raman spectroscopy of an EHMC gel likewise served for initial structural characterization, while short-term physical stability was assessed separately by temperature treatments and centrifugation [73]. Neither study tracked storage changes using repeatedly collected Raman spectra.

5.4. Lipid Oxidation Band Ratios and Sampling Requirements

In specific free-fatty-acid models, Assi et al. [4] used the CH_2/CH_3 band-intensity ratio to discuss hydrogen abstraction and changes in the carbon chain. The authors related the 1165/1640 cm^{-1} band-intensity ratio to changes associated with hydroperoxides and alcohols. They used the 1730/1640 cm^{-1} ratio and trans/cis band ratios to discuss products formed later in oxidation [4]. These wavenumbers identify band positions; the intensity ratios themselves are dimensionless. Interpretation must also consider changes in the denominator: a ratio increases if the denominator band weakens, even when the other band does not strengthen. Overlapping constituents in creams may alter the contributions to individual peaks. Ratios from the original models should therefore not be used directly as universal oxidation criteria for creams.

Raman comparisons require control of excitation wavelength, power, measurement duration, and sampling location to prevent laser heating or photodamage from altering the sample. Point spectra can identify individual crystals, while mapping helps determine their spatial distribution and reduces the risk of missing localized deposits. Oxidation band ratios should be compared with oxidation indicators measured in the same batches at matched time points to determine whether they mainly reflect early reactions or subsequent products. Table 3 summarizes these Raman studies and distinguishes initial characterization from measurements of changes during or after treatment.

6. Fluorescence Spectroscopy

6.1. Interpretation of Fluorescence Intensity and Lifetime

Fluorescence can originate from ingredients, reaction products, or added probes. Intensity depends on concentration, emission efficiency, and optical geometry. Lifetime describes the characteristic decay time of emission intensity after photoexcitation and depends on the molecular environment and quenching. Overlapping emission can be recorded as an excitation–emission matrix (EEM) and decomposed using parallel factor analysis (PARAFAC).

Absorption of excitation or emitted light by the sample causes inner-filter effects, while droplet and particle scattering also alters measured fluorescence intensity. Other influences include pH, target-compound partitioning between phases, and photobleaching during continued irradiation. Measurements should include a formulation blank without the target compound and checks of absorbance and optical geometry. Front-face fluorescence measurements or validated dilution conditions may be appropriate. If dilution changes the molecular environment, lifetimes in the diluted and original samples should be interpreted separately.

6.2. Active Ingredient Content and Carrier Environment

Phanphothong et al. [65] measured melatonin at an excitation wavelength of 274 nm and an emission wavelength of 370 nm, with an HPLC comparison reported in the supplementary material accompanying their article. Encapsulation efficiency in transfersomes and niosomes did not change significantly after six cycles of 24 h at 4 °C followed by 24 h at 45 °C. Encapsulation efficiency is the fraction of the total measured melatonin held inside the carriers. If the encapsulated and total amounts fall in the same proportion, this fraction stays the same. Particle size, PDI, and zeta potential changed markedly in the niosomes despite the unchanged encapsulation efficiency.

A retinol liposome study focused more on the molecular environment. Sumrall et al. measured bulk fluorescence lifetimes with 374 nm excitation, irradiated samples with ultraviolet light at 312 nm, and examined liposomes using fluorescence lifetime imaging microscopy (FLIM) [12]. Without cholesterol, BHT increased the initial lifetime but accelerated the decrease in mean lifetime after irradiation. Adding cholesterol altered this effect of BHT. The lifetime measurements show how the retinol fluorescence response varied with membrane composition and irradiation. They do not measure how much retinol remained.

6.3. Excited-State Mechanisms in Sunscreen Systems

Kawakami et al. [28] exposed sunscreen emulsion films to a UVA dose of 27.5 J/cm^2 and compared the UVA/UVB mean absorbance ratio and HPLC-measured amounts before and after irradiation. Separately, they used steady-state and time-resolved fluorescence to examine avobenzone–DHHB interactions in a methanol model [28]. In methanol, avobenzone emission intensity decreased while its lifetime remained largely unchanged, consistent with static quenching. However, content measurements in the emulsion films did not show improved post-irradiation avobenzone retention with DHHB.

Avobenzone absorption, fluorescence, and lifetime can vary with cyclodextrin inclusion and excimer formation [39]. A p-aminobenzoic acid (PABA)–hydrotalcite study compared free and intercalated samples using the decline in fluorescence during irradiation [66]. Emission in these systems depends on the molecular environment and may also change through photoreactions. Post-irradiation content measurements can help distinguish fluorescence quenching and changes in molecular state from actual filter loss.

6.4. Oxidation-Related Fluorescence and Reactive Oxygen Species Detection

Some carbonyl products of lipid oxidation react with amino compounds to form fluorescent products. Veberg et al. [67] observed effects of aldehyde structure and combinations in aldehyde–amino acid models. Aubourg et al. [68] studied sardines during frozen storage, measuring fluorescence-intensity ratios at two excitation/emission wavelength pairs in extracts. The fluorescence ratio of the aqueous extract was correlated with the thiobarbituric acid (TBA) index [68]. Such fluorescence reflects some subsequent reaction products rather than directly measuring the initial hydroperoxides. In cosmetics, emission will depend on the available reactants, pH, and quenching. The time of signal appearance should also be compared with oxidation indicators in the same samples.

Fluorescent probes can also examine reactions involving reactive oxygen species (ROS) during irradiation. Ibrahim et al. [69] compared TiO_2 with lignin/TiO_2 composites using coumarin as a probe. They monitored emission near 460 nm from 7-hydroxycoumarin, a product formed in reactions involving hydroxyl radicals. During 20–100 min of sunlight exposure, the probe signal from kraft lignin/TiO_2 was lower than that from pure TiO_2 or alkali lignin/TiO_2 [69]. Probe adsorption and competition from other constituents also affect the signal. For formulation assessment, additional measurements of filter content and film protection could establish whether the probe response corresponds to actual changes.

6.5. Decomposition and Assignment of Overlapping Fluorescence

EEM–PARAFAC decomposes overlapping fluorescence signals into mathematical components. The tutorial by Stedmon and Bro [75] on dissolved organic matter provides methodological guidance for this analysis. The model assumes approximately invariant excitation and emission spectral shapes for each component across samples. Aging-related changes in pH, aggregation, or quenching may violate this assumption. After blank correction and treatment of scattering and inner-filter effects, assessment should include residuals, spectral shapes, split-half validation, and fits obtained from different initial values. A fitted component may represent more than one fluorophore. Its score alone cannot define a product failure limit; that would require an independently defined quality limit and evidence linking the score to the measured quality indicator. Table 4 summarizes the fluorescence studies, their reference measurements, and the limits of their conclusions.

7. Study Design and Validation for Combined Spectroscopy

7.1. Combined Measurements and Data Analysis

The studies discussed below show what individual measurements can reveal about lipid oxidation and sunscreen stability. They do not establish whether combining those measurements would detect a change earlier or explain it more clearly than a single method. For lipid oxidation, FTIR or Raman spectra [4,5], NIR estimates of oxidation [59], and fluorescence signals from later reactions [68] could be compared using the same batches at matched time points. Sunscreen studies could combine absorption, excited-state interactions, and chromatographic content measurements [27,28,39]. These paired results would allow comparison of when different signals appear and whether adding a measurement method helps explain the causes of change.

Spectra from different methods can be concatenated directly. Alternatively, band ratios, selected wavelengths, or a small number of summary variables can be extracted and analyzed together. Separate models can also be built and their results combined using predefined rules. Direct concatenation retains more variables but may add redundancy. Feature extraction reduces model size, although it requires checking that information relevant to the changes has not been lost.

7.2. Model Purpose and Independent Testing

Model choice depends on the measurement task. PCA summarizes the main differences among spectral samples and helps identify outliers [76]. PLSR relates spectra to a target indicator for numerical prediction [77]. Partial least squares discriminant analysis (PLS-DA) builds a classification model from known classes [78]. In stability studies, these approaches can examine differences among stored samples, predict content or oxidation indicators, and distinguish predefined sample classes, respectively. If classes represent acceptable and unacceptable samples, they should be defined by the relevant quality requirements and reference measurements, rather than storage time alone.

In the face-cream study, FT-NIR spectra were used to group samples by storage condition [58]. The question is whether similar groups appear in new samples. The fish-oil emulsion and hydrogel studies addressed a different question: how closely did the predicted conjugated diene values [59] or initial ingredient contents [63] agree with the measured values?

Figure 3 illustrates a proposed design for testing whether a model performs well on new batches. Independently prepared batches are assigned either to model development or to testing, with all repeated scans and storage time points from a given batch kept in the same set. During cross-validation, all data-dependent steps, including preprocessing, feature selection, and model tuning, use only the training portion of each fold. The final model and preprocessing procedure are fixed before the held-out batches are tested. Reporting the numbers of batches, samples, and scans separately distinguishes independent batches from repeated measurements. If the model is intended for use on other instruments, its performance also needs to be assessed on those instruments.

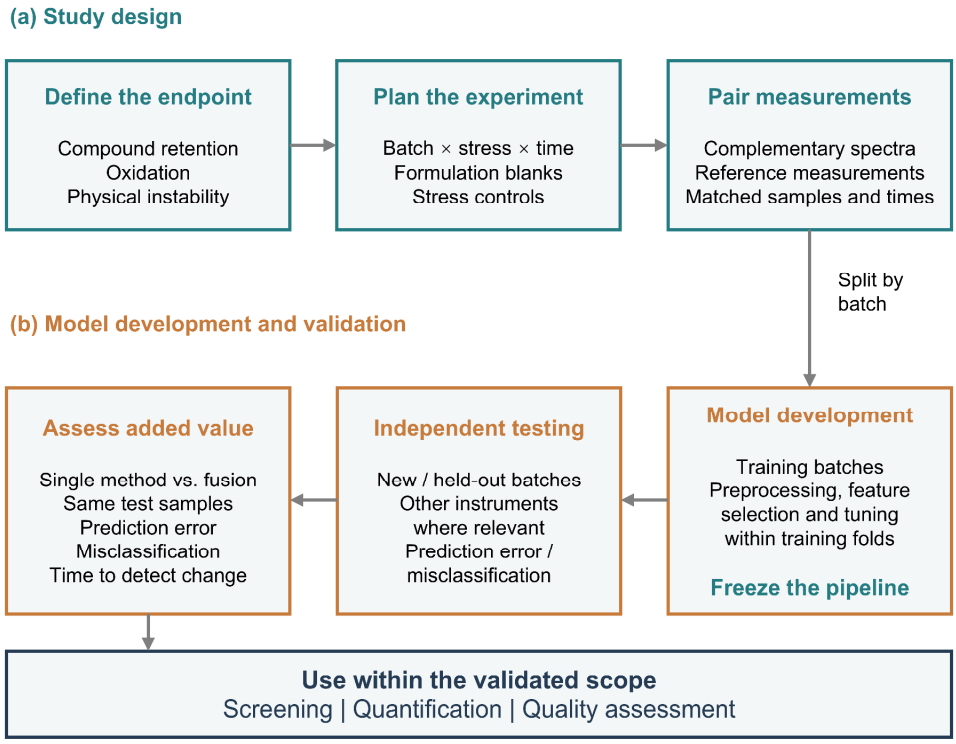

Figure 3. Proposed workflow for comparing combined and single spectroscopic methods on the same samples. Panel (**a**) shows how to pair spectral and reference measurements. Panel (**b**) shows how a model intended for use on new batches could be developed and tested. The workflow is proposed in this review; the cited studies did not evaluate it as a whole.

To assess whether a second spectroscopic method improves performance, the combined model can be compared with each single-method model on the same held-out

samples. For predictions of content or oxidation indicators, prediction error measures the size of the deviations from the reference values, while mean bias indicates whether predictions tend to be too high or too low. For pass/fail decisions, sensitivity and specificity indicate how reliably the model identifies samples in each class. For early detection, the comparison is the time at which each method first detects the change under the same storage or exposure conditions.

7.3. Process Monitoring and Portable Measurements

Applying laboratory spectroscopy to production requires representative sampling, sufficient measurement speed, and assessment of temperature effects under operating conditions. The in situ NIR study of food emulsions [59] offers an approach to direct measurement and modeling, but did not validate use on a cosmetics production line. The face-cream packaging and storage study [58] examined stored samples; its sampling purpose and operating conditions differ from those of process monitoring.

Differences in spectral range, resolution, probe contact, and light source can affect predictions from portable instruments. Calibration transfer or standardization can reduce some instrument differences [79]. Errors in new samples should still be checked after changes in formulation, raw materials, or suppliers.

8. Comparison and Method Selection

Table 5 groups the studies by formulation type and shows what each method measured. It also distinguishes measurements made during storage or irradiation from spectra collected only after preparation.

Table 5. Spectroscopic measurements and their interpretation by formulation type.

Formulation or Sample	Method	What Was Measured	Sampling and Interpretation
Oil-in-water emulsion [5]	FTIR	Changes in lipid unsaturation and carbonyl bands during aging	The carbonyl region includes esters already present in the oil phase. Band changes alone do not quantify newly formed oxidation products.
Ascorbic acid cream [1]	UV–Vis	Ascorbic acid remaining after light exposure, measured at 245 nm in a cream extract	Extraction recovery and the pH of the measurement solution affect the content estimate.
Commercial face cream [58]	FT-NIR and colorimetry	Spectral differences after 2 and 4 months of storage in five container types; correlations with measured color	The spectra distinguished some storage and packaging conditions but did not identify the cause of the differences.
Cosmetic hydrogel [63]	Raman spectroscopy with PLSR	Piperonyl ester content in freshly prepared hydrogels containing 0.4–8.3% (w/w) of the esters	The model was tested on freshly prepared samples. Its accuracy after storage was not established.
Caffeine nanoemulsion [64]	Raman spectroscopy	Molecular fingerprint of the freshly prepared nanoemulsion	Raman spectra were not collected during storage. Appearance, droplet size, and other physical measurements were used to assess subsequent changes.
Sunscreen film [27,31]	UV–Vis	Intact film: optical measurements used to estimate in vitro SPF [31]. Extract of an irradiated film: UVA/UVB mean absorbance ratio [27]	Substrate and spreading affect intact-film measurements. The ratio measured in an extract does not show how much of each filter remains; individual filters were measured by HPLC [27].

Anhydrous foundation [7]	Raman microspectroscopy	Avobenzone-related signals in visible deposits after approximately 2 months of aging	Measurements targeted deposits that had already formed. They helped identify deposit constituents but did not establish when crystallization began.
Retinol liposome dispersion [12]	Fluorescence lifetime spectroscopy and FLIM	Changes in retinol fluorescence lifetime after UV irradiation	Lifetime depends on the surroundings of the emitting molecules and cannot be read directly as the amount of retinol remaining.

8.1. Three Common Measurement Tasks

UV–Vis or fluorescence may be suitable for measuring a target ingredient after storage if its characteristic absorption or fluorescence can be distinguished from other constituents [1,18,65]. Formulation blanks and degraded samples test selectivity, while recovery measurements assess extraction losses. For UV–Vis measurements, pH and scattering should also be controlled. If other compounds absorb at the same wavelengths, a validated HPLC assay that separates the target ingredient from its degradation products can determine how much of the ingredient remains. When the aim is to track the loss of a known active ingredient, UV–Vis measurements supported by a validated HPLC assay may be sufficient; additional structural analysis is needed when the identity of a product or the cause of a spectral change remains unresolved. A different question arises when an absorption band shifts: FTIR provided evidence of an interaction between vitamin C and chitosan [14], while NMR distinguished the keto–enol and diketo forms of avobenzone in model solutions [42]. If the aim is to identify a degradation product, GC–MS or liquid chromatography–mass spectrometry (LC–MS) can provide structural information. For example, Freitas et al. [27] used GC–MS to identify sunscreen photoproducts. NIR and Raman content models likewise require comparison with content obtained by reference measurements.

Transmission, backscattering, or optical measurements along the sample height can identify signs of physical change in emulsions [6,54,55]. Particle sizing and microscopy help determine whether droplet size or distribution has changed, while rheology or conductivity provides additional information on bulk physical properties. Raman microspectroscopy and PXRD can further identify the composition of local crystals [7]. Droplets can aggregate and emulsions can separate even when the functional-group bands remain unchanged. For water-in-oil emulsions, a dilution procedure used for oil-in-water emulsions should first be checked for changes in droplet size or dispersion. For powders, measurements at several sampling points can show whether a spectrum from one location is representative of the sample.

Assessment of sunscreen performance after irradiation requires UV–Vis transmission or absorption measurements using specified substrates, application amounts, and light doses, with in vitro indices reported according to the chosen method. Film thickness, spreading, and scattering are major interferences [44,45]. HPLC, supplemented by mass spectrometry where needed, can determine whether individual filters decrease or photoproducts form [27]. Fluorescence can examine excited-state interactions [28].

Studies of sunscreen photostability illustrate why the size of a spectral change depends on how it is measured. Holt et al. [43] found that changing the proportions of two filters in an oil-phase model altered the loss of in vitro SPF after irradiation. Scalia et al. [44] found a different source of variation: the same commercial products showed larger SPF losses on PMMA plates than on tape, and the measurements on PMMA agreed more closely with HPLC measurements of filter loss. Both studies detected a decline in optical protection, but their percentages address different comparisons and should not be pooled.

Table 6 contrasts these results with applications for which the evidence is limited to a model formulation or a measurement made after aging.

Table 6. Quantitative findings and limits of the evidence for selected applications of spectroscopy in cosmetic stability assessment.

Application	Comparison and Reported Result	What the Evidence Supports
Sunscreen photostability: filter composition [43]	In two oil-phase models with the same avobenzone concentration, reversing the proportions of EHMC and octocrylene changed the post-irradiation SPF loss from 15.8% to 21.3% and the UVA-PF loss from 21.4% to 28.0%.	The blend with more EHMC showed a larger loss of optical protection. These percentages describe changes in protection factors, not the amount of avobenzone lost.
Sunscreen photostability: film substrate [44]	After simulated sunlight exposure, in vitro SPF fell by 31.3–63.1% on PMMA plates and by 10.4–23.8% on Transpore tape for the same set of commercial sunscreens.	On PMMA, reductions in SPF and UVA-PF agreed more closely with HPLC measurements of the corresponding filter losses. Agreement was poorer on tape.
Lipid oxidation in emulsions [5,59]	FTIR tracked changes in unsaturation and carbonyl bands during aging of oil-in-water emulsions [5]. In a separate emulsion containing 20% (v/v) fish oil, NIR predicted the conjugated diene value with a reported error of 7.8% (prediction $R^2 = 0.996$) [59].	FTIR showed the direction of chemical change; the NIR study tested a numerical prediction against an oxidation assay. Its prediction error applies to the fish oil model, not to cosmetic creams.
Retinol in liposomes [12]	Under 312 nm irradiation, mean fluorescence lifetime in cholesterol-free liposomes declined at 0.034 ± 0.006 ns/s without BHT and 0.048 ± 0.008 ns/s with BHT (fitted rates ± standard error).	The rates describe how quickly fluorescence lifetime changed during exposure. They do not give the rate of retinol loss in concentration units.
Raman quantification in hydrogels [63]	A model for piperonyl esters covered 0.4–8.3% (w/w). With 64 training samples and 32 test samples, the prediction error (RMSEP) was 0.148% (w/w).	Quantification was tested in freshly prepared hydrogels. The reported error does not establish accuracy after storage or degradation.
Raman identification of crystals after aging [7]	Visible deposits appeared in an anhydrous foundation after approximately 2 months. Raman analysis of the deposits, together with microscopy and X-ray measurements, helped identify their constituents.	The study identified material in deposits that had already formed. It did not measure the onset or rate of crystallization.

8.2. Spectroscopic Screening and Follow-Up Testing

In quality control or regulatory testing, an unexpected spectrum can flag a sample for further examination. The follow-up test depends on what the spectrum leaves unresolved. In one sunscreen study, the UVA/UVB absorbance ratio of extracts from irradiated films remained relatively high, although HPLC showed losses of individual filters [27]. When the question is how much of a particular filter remains, its content should be measured directly. In an emulsion, a change in backscattering can identify where the sample has changed, while microscopy or droplet sizing can show whether the droplets have grown [6,54,55].

A pass/fail decision requires a defined quality indicator and an applicable limit. A spectroscopic result can support that decision if the method has been validated for the product and indicator in question. When the measurement uncertainty spans the limit, the sample should be checked using an appropriate reference method. A result from a single time point does not establish that the product will meet its specification throughout storage.

9. Conclusions and Outlook

Studies of finished products and experimental formulations have recorded changes in selected active ingredient contents, ultraviolet absorption after irradiation, color, and emulsion physical properties. Crystals in a foundation were identified by Raman spectroscopy after aging, but the measurements did not establish when crystallization

began. Hydrogel content prediction and caffeine nanoemulsion characterization were based on initial Raman spectra, without repeated spectral collection during storage. In one sunscreen study, some filters decreased even though the UVA/UVB absorbance ratio of the extract remained relatively high. In the niosome study, particle properties changed while melatonin encapsulation efficiency showed no significant change.

Three questions remain open. In sunscreens, when does a change in film transmittance first become measurable relative to the loss of an individual UV filter measured by chromatography? In emulsions, can changes in backscattering distinguish droplet growth from redistribution when checked against microscopy at the same sampling heights? In foundations, can repeated Raman measurements at mapped sites detect crystals before they become visible?

Author Contributions: Conceptualization, J.C. and G.-L.W.; investigation, X.-L.C., T.-T.L., X.-R.W. and S.-M.J.; writing—original draft preparation, X.-L.C. and T.-T.L.; writing—review and editing, X.-L.C. and T.-T.L. All authors have read and agreed to the published version of the manuscript.

Funding: This research received no external funding.

Institutional Review Board Statement: Not applicable.

Informed Consent Statement: Not applicable.

Data Availability Statement: No new data were created or analyzed in this study. Data sharing is not applicable to this article.

Conflicts of Interest: The authors declare no conflicts of interest.

Abbreviations

The following abbreviations are used in this manuscript:

ATR	Attenuated total reflectance
BHT	Butylated hydroxytoluene
DHHB	Diethylamino hydroxybenzoyl hexyl benzoate
DLS	Dynamic light scattering
DSC	Differential scanning calorimetry
EDS	Energy-dispersive X-ray spectroscopy
EEM	Excitation–emission matrix
EHMC	Ethylhexyl methoxycinnamate
FLIM	Fluorescence lifetime imaging microscopy
FTIR	Fourier-transform infrared
FT-NIR	Fourier-transform near-infrared
GC–MS	Gas chromatography–mass spectrometry
HEC	Hydroxyethyl cellulose
HPLC	High-performance liquid chromatography
LC–MS	Liquid chromatography–mass spectrometry
LDH	Layered double hydroxide
MIR	Mid-infrared
MS	Mass spectrometry
NIR	Near-infrared
NLC	Nanostructured lipid carrier
NMR	Nuclear magnetic resonance
OMC	Octyl methoxycinnamate
O/W	Oil-in-water
PABA	p-Aminobenzoic acid
PARAFAC	Parallel factor analysis
PCA	Principal component analysis
PDI	Polydispersity index
PE	Piperonyl esters

PLA	Poly(lactic acid)
PLS1	Single-response partial least squares regression
PLS-DA	Partial least squares discriminant analysis
PLSR	Partial least squares regression
PMMA	Poly(methyl methacrylate)
PXRD	Powder X-ray diffraction
RMSEP	Root mean square error of prediction
ROS	Reactive oxygen species
SEM	Scanning electron microscopy
SLN	Solid lipid nanoparticle
SPF	Sun protection factor
TBA	Thiobarbituric acid
TEM	Transmission electron microscopy
TG/DTG	Thermogravimetry/derivative thermogravimetry
UHPLC	Ultra-high-performance liquid chromatography
UVA	Ultraviolet A
UVA-PF	UVA protection factor
UVB	Ultraviolet B
UV–Vis	Ultraviolet–visible
XPS	X-ray photoelectron spectroscopy
XRD	X-ray diffraction

References

1. Ahmad, I.; Sheraz, M.A.; Ahmed, S.; Shaikh, R.H.; Vaid, F.H.M.; Khattak, S.U.R.; Ansari, S.A. Photostability and interaction of ascorbic acid in cream formulations. *AAPS PharmSciTech* **2011**, *12*, 917–923. https://doi.org/10.1208/s12249-011-9659-1.
2. Dondi, D.; Albini, A.; Serpone, N. Interactions between different solar UVB/UVA filters contained in commercial suncreams and consequent loss of UV protection. *Photochem. Photobiol. Sci.* **2006**, *5*, 835–843. https://doi.org/10.1039/B606768A.
3. Lhiaubet-Vallet, V.; Marin, M.; Jimenez, O.; Gorchs, O.; Trullas, C.; Miranda, M.A. Filter-filter interactions. Photostabilization, triplet quenching and reactivity with singlet oxygen. *Photochem. Photobiol. Sci.* **2010**, *9*, 552–558. https://doi.org/10.1039/B9PP00158A.
4. Assi, A.; Michael-Jubeli, R.; Baillet-Guffroy, A.; Tfayli, A. Characterization of free fatty acids photo-oxidation under UV radiations: A stepwise Raman study. *J. Raman Spectrosc.* **2023**, *54*, 24–36. https://doi.org/10.1002/jrs.6449.
5. Masmoudi, H.; Le Dréau, Y.; Piccerelle, P.; Kister, J. The evaluation of cosmetic and pharmaceutical emulsions aging process using classical techniques and a new method: FTIR. *Int. J. Pharm.* **2005**, *289*, 117–131. https://doi.org/10.1016/j.ijpharm.2004.10.020.
6. Celis, M.-T.; Garcia-Rubio, L.H. Characterization of emulsions: A systematic spectroscopy study. *J. Dispers. Sci. Technol.* **2008**, *29*, 20–26. https://doi.org/10.1080/01932690701686775.
7. Goral, O.; Zukowska, G.Z.; Zero, E.; Siekierski, M.; Krzton-Maziopa, A. Understanding avobenzone crystallization in sunscreen formulations: Role of metal oxide-driven nucleation and stabilization strategies. *Crystals* **2024**, *14*, 663. https://doi.org/10.3390/cryst14070663.
8. Guo, X.; Chen, M.; Meng, X.; Lü, Y.; Zhang, N.; Lian, X.; Wang, C.; Gao, H.; Ma, Q. Research progress in sample pretreatment and analytical techniques for cosmetics. *Chin. J. Chromatogr.* **2020**, *38*, 151–161. https://doi.org/10.3724/SP.J.1123.2019.06031. (In Chinese)
9. Celeiro, M.; Garcia-Jares, C.; Llompart, M.; Lores, M. Recent advances in sample preparation for cosmetics and personal care products analysis. *Molecules* **2021**, *26*, 4900. https://doi.org/10.3390/molecules26164900.
10. Zhao, C.; Zhao, C.; Liu, Y.; Pei, X.; Li, S.; Meng, H.; He, Y. Mechanism and applications of Raman spectroscopy in cosmetics. *J. Raman Spectrosc.* **2026**, *57*, 899–918. https://doi.org/10.1002/jrs.70112.
11. Li, L.; Wang, J.-S.; Ke, L.-N.; Wei, N.-Y.; Wang, H.-Y.; Wang, G.-L. Progress in the application of Raman spectroscopy to cosmetic analysis: From component detection to transdermal mechanism research. *Cosmetics* **2026**, *13*, 79. https://doi.org/10.3390/cosmetics13020079.
12. Sumrall, L.; Smith, L.; Alhatmi, E.; Chmykh, Y.; Mitchell, D.; Nadeau, J. Stability of retinol in liposomes as measured by fluorescence lifetime spectroscopy and FLIM. *BBA Adv.* **2023**, *3*, 100088. https://doi.org/10.1016/j.bbadva.2023.100088.

13. Thewanjutiwong, S.; Phokasem, P.; Disayathanoowat, T.; Juntrapirom, S.; Kanjanakawinkul, W.; Chaiyana, W. Development of film-forming gel formulations containing royal jelly and honey aromatic water for cosmetic applications. *Gels* **2023**, *9*, 816. https://doi.org/10.3390/gels9100816.
14. Liu, L.; Li, K.; Ding, H.; Lv, J.; Zhang, J. Study on preparation of a chitosan/vitamin C complex and its properties in cosmetics. *Nat. Prod. Commun.* **2020**, *15*, 1934578X20946876. https://doi.org/10.1177/1934578X20946876.
15. Sliem, M.A.; Karas, R.A.; Harith, M.A. A promising protected ascorbic acid-hydroxyapatite nanocomposite as a skin anti-ager: A detailed photo- and thermal stability study. *J. Photochem. Photobiol. B Biol.* **2017**, *173*, 661–671. https://doi.org/10.1016/j.jphotobiol.2017.07.004.
16. Kim, H.; Hu, Y.; Jeong, D.; Jun, B.-H.; Cho, E.; Jung, S. Synthesis, characterization, and retinol stabilization of fatty amide-β-cyclodextrin conjugates. *Molecules* **2016**, *21*, 963. https://doi.org/10.3390/molecules21070963.
17. Saleem, R.; Rehman, M.; Ahmed Khan, T.; Khalid, Q.; Ahmad, A.; Awais, M.; Ahmad, A.; Ijaz, S. Tretinoin loaded NLCs-based sunscreen cream; preparation and characterization. *Pak. J. Pharm. Sci.* **2025**, *38*, 315–323. https://doi.org/10.36721/pjps.2025.38.1.reg.315-323.1.
18. Arkan Yousif, H.; Al-Ani, I.; Hajleh, M.N.A.; Matalqah, S.; Dayyih, W.A.; Al-Dujaili, E.A. Preparation and evaluation of complexed ubiquinone (coenzyme Q10) antiaging hyaluronic acid–vitamin C serum for skin care. *J. Cosmet. Dermatol.* **2025**, *24*, e16706. https://doi.org/10.1111/jocd.16706.
19. Ameri, A.; Khazaeli, P.; Behnam, B.; Mehrabani, M.; Forootanfar, H. Formulation and optimization of phytosomes of ethanolic extract of Viola tricolor flowers using design of experiment (DOE) to evaluate in vitro photoprotective potential as sunscreen cream. *Ind. Crops Prod.* **2024**, *209*, 118057. https://doi.org/10.1016/j.indcrop.2024.118057.
20. Wang, J.; Tang, J.; Zhou, X.; Xia, Q. Physicochemical characterization, identification and improved photo-stability of alpha-lipoic acid-loaded nanostructured lipid carrier. *Drug Dev. Ind. Pharm.* **2014**, *40*, 201–210. https://doi.org/10.3109/03639045.2012.753901.
21. Brand-Williams, W.; Cuvelier, M.E.; Berset, C. Use of a free radical method to evaluate antioxidant activity. *LWT-Food Sci. Technol.* **1995**, *28*, 25–30. https://doi.org/10.1016/S0023-6438(95)80008-5.
22. Re, R.; Pellegrini, N.; Proteggente, A.; Pannala, A.; Yang, M.; Rice-Evans, C. Antioxidant activity applying an improved ABTS radical cation decolorization assay. *Free Radic. Biol. Med.* **1999**, *26*, 1231–1237. https://doi.org/10.1016/S0891-5849(98)00315-3.
23. Dahmen, I.; Chtourou, H.; Hadrich, F.; Baccar, N.; Sayadi, S.; Ayadi, H.; Chamkha, M. Phormidium versicolor PC skin cream evaluation for its stability and biological activities. *Appl. Microbiol. Biotechnol.* **2024**, *108*, 541. https://doi.org/10.1007/s00253-024-13359-0.
24. Yang, W.; Gong, Y.; Wang, Y.; Wu, C.; Zhang, X.; Li, J.; Wu, D. Design of gum Arabic/gelatin composite microcapsules and their cosmetic applications in encapsulating tea tree essential oil. *RSC Adv.* **2024**, *14*, 4880–4889. https://doi.org/10.1039/d3ra08526k.
25. Serpone, N.; Salinaro, A.; Emeline, A.V.; Horikoshi, S.; Hidaka, H.; Zhao, J. An in vitro systematic spectroscopic examination of the photostabilities of a random set of commercial sunscreen lotions and their chemical UVB/UVA active agents. *Photochem. Photobiol. Sci.* **2002**, *1*, 970–981. https://doi.org/10.1039/B206338G.
26. Damiani, E.; Rosati, L.; Castagna, R.; Carloni, P.; Greci, L. Changes in ultraviolet absorbance and hence in protective efficacy against lipid peroxidation of organic sunscreens after UVA irradiation. *J. Photochem. Photobiol. B Biol.* **2006**, *82*, 204–213. https://doi.org/10.1016/j.jphotobiol.2005.03.011.
27. Freitas, J.V.; Lopes, N.P.; Gaspar, L.R. Photostability evaluation of five UV-filters, trans-resveratrol and beta-carotene in sunscreens. *Eur. J. Pharm. Sci.* **2015**, *78*, 79–89. https://doi.org/10.1016/j.ejps.2015.07.004.
28. Kawakami, C.M.; Máximo, L.N.C.; Fontanezi, B.B.; da Silva, R.S.; Gaspar, L.R. Diethylamino hydroxybenzoyl hexyl benzoate (DHHB) as additive to the UV filter avobenzone in cosmetic sunscreen formulations—Evaluation of the photochemical behavior and photostabilizing effect. *Eur. J. Pharm. Sci.* **2017**, *99*, 299–309. https://doi.org/10.1016/j.ejps.2016.12.031.
29. Silva, G.C.; Rodrigues, R.A.F.; Bottoli, C.B.G. Formulation stability of sunscreens with passion fruit seed and paracress extracts. *J. Braz. Chem. Soc.* **2025**, *36*, e-20250132. https://doi.org/10.21577/0103-5053.20250132.
30. Vettor, M.; Perugini, P.; Scalia, S.; Conti, B.; Genta, I.; Modena, T.; Pavanetto, F. Poly(D,L-lactide) nanoencapsulation to reduce photoinactivation of a sunscreen agent. *Int. J. Cosmet. Sci.* **2008**, *30*, 219–227. https://doi.org/10.1111/j.1468-2494.2008.00443.x.
31. Cozzi, A.C.; Perugini, P.; Gourion-Arsiquaud, S. Comparative behavior between sunscreens based on free or encapsulated UV filters in term of skin penetration, retention and photo-stability. *Eur. J. Pharm. Sci.* **2018**, *121*, 309–318. https://doi.org/10.1016/j.ejps.2018.06.001.

32. Wang, K.; Zhang, Q.-J.; Miao, Y.-L.; Luo, S.-Q.; Wang, H.-C.; Zhang, W.-P. Effect of solid lipid's structure on nanostructured lipid carriers encapsulated with sun filter: Characterisation, photo-stability and in vitro release. *J. Microencapsul.* **2017**, *34*, 104–110. https://doi.org/10.1080/02652048.2017.1290156.
33. Caldas, A.R.; Faria, M.J.; Ribeiro, A.; Machado, R.; Gonçalves, H.; Gomes, A.C.; Soares, G.M.B.; Lopes, C.M.; Lúcio, M. Avobenzone-loaded and omega-3-enriched lipid formulations for production of UV blocking sunscreen gels and textiles. *J. Mol. Liq.* **2021**, *342*, 116965. https://doi.org/10.1016/j.molliq.2021.116965.
34. Ambrogi, V.; Latterini, L.; Marmottini, F.; Pagano, C.; Ricci, M. Mesoporous silicate MCM-41 as a particulate carrier for octyl methoxycinnamate: Sunscreen release and photostability. *J. Pharm. Sci.* **2013**, *102*, 1468–1475. https://doi.org/10.1002/jps.23478.
35. Perioli, L.; Nocchetti, M.; Ambrogi, V.; Latterini, L.; Rossi, C.; Costantino, U. Sunscreen immobilization on ZnAl-hydrotalcite for new cosmetic formulations. *Microporous Mesoporous Mater.* **2008**, *107*, 180–189. https://doi.org/10.1016/j.micromeso.2007.02.021.
36. Al-Rawashdeh, N.A.F.; Al-Sadeh, K.S.; Al-Bitar, M.-B. Physicochemical study on microencapsulation of hydroxypropyl-β-cyclodextrin in dermal preparations. *Drug Dev. Ind. Pharm.* **2010**, *36*, 688–697. https://doi.org/10.3109/03639040903449738.
37. Yuan, L.; Li, S.; Huo, D.; Zhou, W.; Wang, X.; Bai, D.; Hu, J. Studies on the preparation and photostability of avobenzone and (2-hydroxy)propyl-β-cyclodextrin inclusion complex. *J. Photochem. Photobiol. A Chem.* **2019**, *369*, 174–180. https://doi.org/10.1016/j.jphotochem.2018.09.036.
38. d'Agostino, S.; Azzali, A.; Casali, L.; Taddei, P.; Grepioni, F. Environmentally friendly sunscreens: Mechanochemical synthesis and characterization of β-CD inclusion complexes of avobenzone and octinoxate with improved photostability. *ACS Sustain. Chem. Eng.* **2020**, *8*, 13215–13225. https://doi.org/10.1021/acssuschemeng.0c02735.
39. Vishwakarma, J.; Takkella, D.; Sharma, S.; Gavvala, K. Modulation of excimer formation and photostability of avobenzone inside the nanocavities of cyclodextrins. *J. Photochem. Photobiol. A Chem.* **2024**, *449*, 115411. https://doi.org/10.1016/j.jphotochem.2023.115411.
40. Karpkird, T.; Khunsakorn, R.; Noptheeranuphap, C.; Jettanasen, J. Photostability of water-soluble inclusion complexes of UV-filters and curcumin with gamma-cyclodextrin polymer. *J. Incl. Phenom. Macrocycl. Chem.* **2016**, *84*, 121–128. https://doi.org/10.1007/s10847-015-0589-5.
41. Ambrogi, V.; Perioli, L.; Marmottini, F.; Latterini, L.; Rossi, C.; Costantino, U. Mesoporous silicate MCM-41 containing organic ultraviolet ray absorbents: Preparation, photostability and in vitro release. *J. Phys. Chem. Solids* **2007**, *68*, 1173–1177. https://doi.org/10.1016/j.jpcs.2007.02.033.
42. Kuroda, C.; Tsuchida, T.; Tsunoda, C.; Minamide, M.; Hiroshige, R.; Goto, S. Stability and properties of ultraviolet filter avobenzone under its diketo/enol tautomerization induced by molecular encapsulation with β-cyclodextrin. *Langmuir* **2025**, *41*, 1429–1445. https://doi.org/10.1021/acs.langmuir.4c04108.
43. Holt, E.L.; Rodrigues, N.d.N.; Cebrián, J.; Stavros, V.G. Determining the photostability of avobenzone in sunscreen formulation models using ultrafast spectroscopy. *Phys. Chem. Chem. Phys.* **2021**, *23*, 24439–24448. https://doi.org/10.1039/d1cp03610f.
44. Scalia, S.; Mezzena, M.; Bianchi, A. Comparative evaluation of different substrates for the in vitro determination of sunscreen photostability: Spectrophotometric and HPLC analyses. *Int. J. Cosmet. Sci.* **2010**, *32*, 55–64. https://doi.org/10.1111/j.1468-2494.2009.00536.x.
45. Akrman, J.; Kubáč, L.; Bendová, H.; Jírová, D.; Kejlová, K. Quartz plates for determining sun protection in vitro and testing photostability of commercial sunscreens. *Int. J. Cosmet. Sci.* **2009**, *31*, 119–129. https://doi.org/10.1111/j.1468-2494.2008.00482.x.
46. Sharma Bora, N.; Mazumder, B.; Patowary, P.; Kishor, S.; Doma Bhutia, Y.; Chattopadhyay, P.; Dwivedi, S.K. Formulation development and accelerated stability testing of a novel sunscreen cream for ultraviolet radiation protection in high altitude areas. *Drug Dev. Ind. Pharm.* **2019**, *45*, 1332–1341. https://doi.org/10.1080/03639045.2019.1616750.
47. Patil, A.; Masareddy, R.S.; Patil, A.S.; Dwivedi, P.S.R. Microsponge gel approach to increase the stability and efficacy of avobenzone as a sun-protective agent. *J. Pharm. Innov.* **2022**, *17*, 1347–1359. https://doi.org/10.1007/s12247-021-09616-8.
48. Gao, M.; He, L.; Hu, M.; Zhang, Y.-R.; Zhu, Y. Study on the aging of carminic acid by UV-vis spectrophotometry. *J. Hunan Univ. (Nat. Sci.)* **2013**, *40*, 83–86 (In Chinese)
49. Tan, P.; Cui, H.; Jiang, C.; Jiang, C.; Huang, Q.; Li, J.; Tang, Y.; Feng, Y. Preparation and optimization of pickering emulsion stabilized by organosilane-modified palygorskite to encapsulate natural colorants for cosmetic application. *Appl. Clay Sci.* **2025**, *276*, 107954. https://doi.org/10.1016/j.clay.2025.107954.
50. Liu, X.; Cao, L.; Jiang, C.; Wang, H.; Zhang, X.; Liu, Q.; Li, H.; Tang, Y.; Feng, Y. Fabrication of multifunctional hybrid pigment for color cosmetics based on chitosan-modified palygorskite and sappanwood extract. *Int. J. Biol. Macromol.* **2024**, *279*, 135259. https://doi.org/10.1016/j.ijbiomac.2024.135259.

51. Wang, R.; Zhang, S.; Zhang, X.; Liu, Q. Preparation of hydrophobic layered double hydroxide-based composite pigments via octyltriethoxysilane surface modification for cosmetic applications. *Dalton Trans.* **2024**, *53*, 9406–9415. https://doi.org/10.1039/d4dt00531g.
52. Zhang, S.; Tang, Y.; Wang, R.; Liu, Q.; Zhang, X.; Zhao, H. Design of hydrophobic zein/dye-LDHs biohybrid pigments for cosmetic applications. *Appl. Clay Sci.* **2024**, *250*, 107256. https://doi.org/10.1016/j.clay.2024.107256.
53. Srisawang, N.; In-na, P.; Poompradub, S. Natural pigments from micro- and macro-algae for nail polish application. *Algal Res.* **2025**, *88*, 103983. https://doi.org/10.1016/j.algal.2025.103983.
54. Ji, Z.; Tang, Y.; Wang, C.; Yang, J. Preparation of submicron capsules containing fragrance and their application as emulsifier. *Polym. Bull.* **2021**, *78*, 1821–1833. https://doi.org/10.1007/s00289-020-03186-4.
55. Lixandru Matei, I.L.; Sava, B.A.; Ionescu, A.I.; Sarosi, C.; Vasilievici, G.; Băjan, M.; Movileanu, D.L.; Popovici, D.R.; Baiounf, A. Retinol dispersion in the form of hydrogel for dermal delivery. *Stud. Univ. Babeș-Bolyai Chem.* **2025**, *70*, 37–51. https://doi.org/10.24193/subbchem.2025.2.03.
56. Cruz-Lugo, A.; Rivera-Santiago, S.V.; Cortés-Norat, A.S.; Rosario-Isona, V.I.; Nieves-Moron, S.V.; Viera-Sánchez, V.V.; Díaz-Vázquez, L.M. Photoprotective and antioxidant liposomal formulations from Sargassum-derived biomolecules for skincare applications. *ACS Omega* **2025**, *10*, 52018–52031. https://doi.org/10.1021/acsomega.5c09406.
57. Kim, Y.S.; Park, J.H.; Bae, Y.H. Degradation and stabilization of cosmetic polyetherurethane in alcoholic solution. *J. Appl. Polym. Sci.* **2003**, *89*, 2270–2276. https://doi.org/10.1002/app.12407.
58. Gliszczyńska-Świgło, A.; Nowak, P.; Dobrucka, R.; Pawlak-Lemańska, K. The influence of packaging on cosmetic emulsion during storage assessed by FT-NIR spectroscopy and color measurements. *J. Cosmet. Sci.* **2018**, *69*, 245–255.
59. Daoud, S.; Waschatko, G.; Bou-Maroun, E.; Cayot, P. Fast, direct and in situ monitoring of lipid oxidation in an oil-in-water emulsion by near infrared spectroscopy. *Anal. Methods* **2020**, *12*, 3098–3105. https://doi.org/10.1039/d0ay00583e.
60. Bezerra, G.S.N.; Pereira, M.A.V.; Ostrosky, E.A.; Barbosa, E.G.; de Moura, M.F.V.; Ferrari, M.; Aragão, C.F.S.; Gomes, A.P.B. Compatibility study between ferulic acid and excipients used in cosmetic formulations by TG/DTG, DSC and FTIR. *J. Therm. Anal. Calorim.* **2017**, *127*, 1683–1691. https://doi.org/10.1007/s10973-016-5654-9.
61. Failloux, N.; Bonnet, I.; Perrier, E.; Baron, M.-H. Effects of light, oxygen and concentration on vitamin A1. *J. Raman Spectrosc.* **2004**, *35*, 140–147. https://doi.org/10.1002/jrs.1116.
62. Darvin, M.E.; Sterry, W.; Lademann, J. Resonance Raman spectroscopy as an effective tool for the determination of antioxidative stability of cosmetic formulations. *J. Biophoton.* **2010**, *3*, 82–88. https://doi.org/10.1002/jbio.200910060.
63. Elderderi, S.; Bonnier, F.; Perse, X.; Byrne, H.J.; Yvergnaux, F.; Chourpa, I.; Elbashir, A.A.; Munnier, E. Label-free quantification of nanoencapsulated piperonyl esters in cosmetic hydrogels using Raman spectroscopy. *Pharmaceutics* **2023**, *15*, 1571. https://doi.org/10.3390/pharmaceutics15061571.
64. Freire, T.B.; Dario, M.F.; Mendes, O.G.; de Oliveira, A.C.; Vetore Neto, A.; de Faria, D.L.A.; e Silva, V.R.L.; Baby, A.R.; Velasco, M.V.R. Nanoemulsion containing caffeine for cellulite treatment: Characterization and in vitro evaluation. *Braz. J. Pharm. Sci.* **2019**, *55*, e18236. https://doi.org/10.1590/s2175-97902019000218236.
65. Phanphothong, P.; Kanpipit, N.; Thapphasaraphong, S. The characteristics and biological activity enhancements of melatonin encapsulations for skin care product applications. *Int. J. Pharm. X* **2023**, *6*, 100217. https://doi.org/10.1016/j.ijpx.2023.100217.
66. Perioli, L.; Ambrogi, V.; Bertini, B.; Ricci, M.; Nocchetti, M.; Latterini, L.; Rossi, C. Anionic clays for sunscreen agent safe use: Photoprotection, photostability and prevention of their skin penetration. *Eur. J. Pharm. Biopharm.* **2006**, *62*, 185–193. https://doi.org/10.1016/j.ejpb.2005.08.001.
67. Veberg, A.; Vogt, G.; Wold, J.P. Fluorescence in aldehyde model systems related to lipid oxidation. *LWT-Food Sci. Technol.* **2006**, *39*, 562–570. https://doi.org/10.1016/j.lwt.2005.03.009.
68. Aubourg, S.P.; Sotelo, C.G.; Pérez-Martín, R. Assessment of quality changes in frozen sardine (Sardina pilchardus) by fluorescence detection. *J. Am. Oil Chem. Soc.* **1998**, *75*, 575–580. https://doi.org/10.1007/s11746-998-0068-x.
69. Ibrahim, M.N.M.; Iqbal, A.; Shen, C.C.; Bhawani, S.A.; Adam, F. Synthesis of lignin based composites of TiO_2 for potential application as radical scavengers in sunscreen formulation. *BMC Chem.* **2019**, *13*, 17. https://doi.org/10.1186/s13065-019-0537-3.
70. Smith, B.C. *Fundamentals of Fourier Transform Infrared Spectroscopy*, 2nd ed.; CRC Press: Boca Raton, FL, USA, 2011. https://doi.org/10.1201/b10777.
71. Virkutyte, J.; Al-Abed, S.R.; Dionysiou, D.D. Depletion of the protective aluminum hydroxide coating in TiO_2-based sunscreens by swimming pool water ingredients. *Chem. Eng. J.* **2012**, *191*, 95–103. https://doi.org/10.1016/j.cej.2012.02.074.
72. Cho, E.C.; Kang, S.W. Hydroxyethyl cellulose as carbohydrate polymer scaffold for surfactant-free serums with enhanced hydration and structural stability. *Int. J. Biol. Macromol.* **2026**, *369*, 152785. https://doi.org/10.1016/j.ijbiomac.2026.152785.

73. Li, Z.; Liang, Y.; Liu, C.; Wang, W.; Li, Y.; Du, Z.; Lin, L.; Zhang, J.; Jiang, L.; Xie, L.; et al. Dextrin palmitate and disteardimonium hectorite construct a gel-like EHMC matrix: Enhanced UVB photoprotection and plasma exposure modulation. *Gels* **2026**, *12*, 561. https://doi.org/10.3390/gels12070561.
74. Larkin, P. *Infrared and Raman Spectroscopy: Principles and Spectral Interpretation*, 1st ed.; Elsevier: Boston, MA, USA, 2011. https://doi.org/10.1016/c2010-0-68479-3.
75. Stedmon, C.A.; Bro, R. Characterizing dissolved organic matter fluorescence with parallel factor analysis: A tutorial. *Limnol. Oceanogr. Methods* **2008**, *6*, 572–579. https://doi.org/10.4319/lom.2008.6.572.
76. Beattie, J.R.; Esmonde-White, F.W.L. Exploration of principal component analysis: Deriving principal component analysis visually using spectra. *Appl. Spectrosc.* **2021**, *75*, 361–375. https://doi.org/10.1177/0003702820987847.
77. Wold, S.; Sjöström, M.; Eriksson, L. PLS-regression: A basic tool of chemometrics. *Chemom. Intell. Lab. Syst.* **2001**, *58*, 109–130. https://doi.org/10.1016/s0169-7439(01)00155-1.
78. Ballabio, D.; Consonni, V. Classification tools in chemistry. Part 1: Linear models. *PLS-DA. Anal. Methods* **2013**, *5*, 3790–3798. https://doi.org/10.1039/C3AY40582F.
79. Feudale, R.N.; Woody, N.A.; Tan, H.; Myles, A.J.; Brown, S.D.; Ferré, J. Transfer of multivariate calibration models: A review. *Chemom. Intell. Lab. Syst.* **2002**, *64*, 181–192. https://doi.org/10.1016/S0169-7439(02)00085-0.

Disclaimer/Publisher's Note: The statements, opinions and data contained in all publications are solely those of the individual author(s) and contributor(s) and not of MDPI and/or the editor(s). MDPI and/or the editor(s) disclaim responsibility for any injury to people or property resulting from any ideas, methods, instructions or products referred to in the content.